

Lab on a Chip

Accepted Manuscript



This is an *Accepted Manuscript*, which has been through the Royal Society of Chemistry peer review process and has been accepted for publication.

Accepted Manuscripts are published online shortly after acceptance, before technical editing, formatting and proof reading. Using this free service, authors can make their results available to the community, in citable form, before we publish the edited article. We will replace this *Accepted Manuscript* with the edited and formatted *Advance Article* as soon as it is available.

You can find more information about *Accepted Manuscripts* in the [Information for Authors](#).

Please note that technical editing may introduce minor changes to the text and/or graphics, which may alter content. The journal's standard [Terms & Conditions](#) and the [Ethical guidelines](#) still apply. In no event shall the Royal Society of Chemistry be held responsible for any errors or omissions in this *Accepted Manuscript* or any consequences arising from the use of any information it contains.

Cite this: DOI: 10.1039/xxxxxxxxxx

Leak-tight vertical membrane microvalves[†]

Jonas Hansson,^{a‡} Mikael Hillmering,^{a‡} Tommy Haraldsson,^{*a} and Wouter van der Wijngaart^a

Received Date
Accepted Date

DOI: 10.1039/xxxxxxxxxx

www.rsc.org/journalname

Pneumatic microvalves are fundamental control components in a large range of microfluidic applications. Their key performance parameters are small size, i.e. occupying a minimum of microfluidic real estate, low flow resistance in the open state, and leak-tight closing at limited control pressures. In this work we present the successful design, realization and evaluation of the first leak-tight, vertical membrane, pneumatic microvalves. The realization of the vertical membrane microvalves is enabled by a novel dual-sided molding method for microstructuring monolithic 3D microfluidic networks in PDMS in a single step, eliminating the need for layer-to-layer alignment during bonding. We demonstrate minimum lateral device features down to 20–30 μm in size, and vertical via density of ~ 30000 per cm^2 , which provides significant gains in chip real estate compared to previously reported PDMS manufacturing methods. In contrast to horizontal membrane microvalves, there are no manufacturing restrictions on the cross-sectional geometry of the flow channel of the vertical membrane microvalves. This allows tuning the design towards lower closing pressure or lower open state flow resistance compared to those of horizontal membrane microvalves.

1 Introduction

For many microfluidic devices effective valving is essential, e.g. for large scale integration^{1,2}, pneumatic logic^{3,4}, and compact sample handling systems in heterogeneously integrated devices^{5,6}. Consequently, many different types of microvalves have been developed for Lab-on-a-Chip (LoC) applications, as reviewed in^{7,8}. The valves discussed in this paper are active, externally controlled, normally open pneumatic microvalves. Normally open pneumatic microvalves have become one of the most common microvalve types⁷, due to their ease of manufacturing in polydimethylsiloxane (PDMS) or other rubbery materials^{9,10}.

Normally open pneumatic microvalves consist of two channels, one flow channel and one pneumatic control channel, that are separated by a thin membrane. When the control channel is pressurized the membrane deflects, closing the flow channel. Microfluidic systems are commonly manufactured as 2D microchannel networks. Compared to the plane of the microchannel network, which we will define as horizontal, valve membranes can be positioned horizontally or vertically.

In horizontal membrane microvalves, the flow channel and control channel are typically manufactured in separate mi-

crochannel layers, positioned on top of each other¹¹. To improve the leak-tightness of the horizontal membrane microvalves, the flow channel cross-section is typically semicircular.

Vertical membranes microvalves were first introduced by Sundararajan et al.¹² with the aim to allow both flow and control channels to be microstructured in the same layer. Despite several efforts^{12–14}, vertical membrane valves have failed to be fully closed, due to restrictions to the mechanical deformability of the membrane at its square corners¹⁴. Hence, vertical membranes microfluidic actuators are not being labeled as a “true valve”⁷. Instead, the vertical membrane actuators are used as variable flow resistors¹⁵, mixers¹², droplet generators¹⁶, droplet manipulators^{17,18}, focusing microlenses¹⁹, and particle traps²⁰. In horizontal valve systems, such limit in membrane deformability is compensated by rounded flow channel cross-sections¹¹. In vertical valve systems, the need for demolding the channel during manufacturing has until now not allowed similar geometrical adaptations.

In this paper, we introduce the first vertical membrane valve that can be fully closed. We present the valve design as well as a novel manufacturing technique that enables its realization in a single microstructured layer. We test the limits and possibilities of this manufacturing technique. We demonstrate a few variations of the valve design and investigate their performance through modelling and experiments in terms of control pressure, flow conductance, and leak-tightness.

^a KTH Royal Institute of Technology, Micro and Nanosystems, Osquldas vag 10, 100 44 Stockholm, Sweden, *E-mail: tommyhar@kth.se

[†] Electronic Supplementary Information (ESI) available: [details of any supplementary information available should be included here]. See DOI: 10.1039/b000000x/

[‡] These authors contributed equally to this work

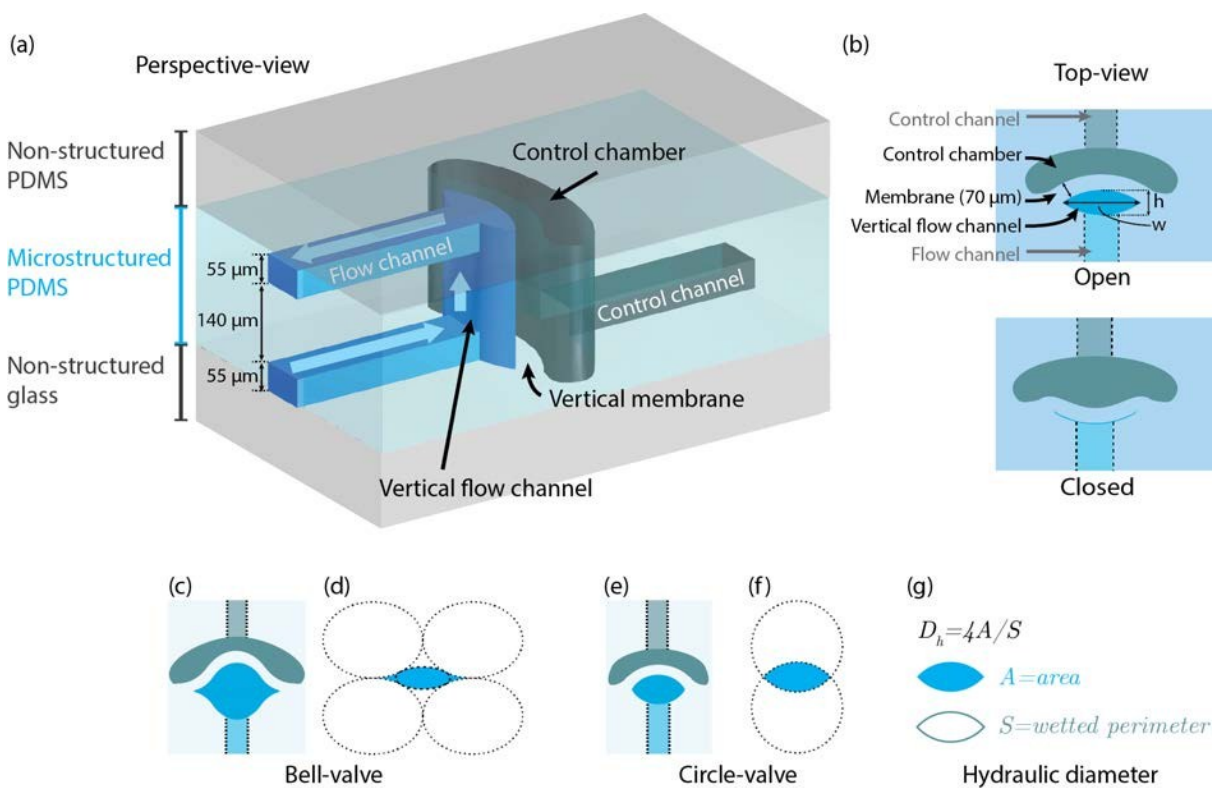


Fig. 1 Vertical valve design. The general valve design is illustrated by (a) 3D rendering, and (b) cross-sectional top view to illustrate the open and closed states. The two types of cross-sectional geometries: (c-d) bell-valve, and (e-f) circle valve, illustrated by top cross-sectional view of the valves (c and e), and cross-sectional design principle of the vertical flow channels (d and f). (g) Definition of hydraulic diameter, D_h illustrated for a circle valve.

2 Valve Design

In our novel approach, we employ 3D microchannel design, which allows a high degree of freedom in designing the cross-sectional shape of vertical channel sections. We designed vertical channels with rounded cross-sectional geometries, similar to those used in horizontal valve designs, to accomplish vertical membrane valves with leakage tight closure (Figure 1). Our novel manufacturing technology with automatic alignment allows valve manufacturing in a single microstructured layer.

The vertical flow channels were designed with two different cross-sectional geometries, where each geometry was manufactured in three different sizes to vary the fluidic resistance of the valve. The first cross-sectional geometry, hereafter referred to as *bell valve*, has a shape defined by two bell-shaped sections (Figure 1, c-d). The bell-shape constitutes smoothly tapered channel edges, designed to reduce the material strain in the membrane edge during deformation with the aim to reduce the required closing pressure. The second cross-sectional geometry, hereafter referred to as *circle valve*, has a shape defined by two sections of a circle (Figure 1, e-f). The circle-valve channel shape is more similar to that of horizontal valves molded on reflowed photoresist. In comparison to the bell valve, the circle valves feature a larger hydrodynamic diameter, $D_h = 4A/S$, for a given channel width (see Figure 1g) with the aim to reduce the fluidic resistance of the flow channel. The geometric details are provided in Table 1. For a complementary graphical overview on how this design differs from previous vertical membrane microvalves and horizontal

membrane microvalves see Table S1 in ESI†.

Symbols for parameters and constants used throughout the paper are summarized in Table S2 in ESI†.

3 Manufacturing

To realize our design in a single microstructured layer, novel manufacturing techniques were developed. Microstructuring the 3D valve design in a single layer provides two main manufacturing challenges: alignment of the two mold sides, and vertical channel (“via”) formation. The manufacturing technique builds on our previous manufacturing development^{21–23}. Here, we describe the manufacturing technique in detail for the first time, and characterize the limits of the manufacturing technique in terms of its alignment and miniaturization.

The manufacturing technique employs two key features: self-aligning double-sided molds, and a smart surface coating. The self-aligning double-sided molds features guiding pins and guiding frames that interlocks when pressed together (see Figure 2). The smart surface coating is 75 nm thick and features reactive amine groups and PVA. The reactive amine groups ensure open vertical vias by depletion of the PDMS polymerization catalyst locally where the mold features are pressed together.²⁴ PVA is water dissolvable and hence allows low-stress mold release and transfer, which is especially important for thin and fragile structures.²¹ The manufacturing steps are depicted in Figure 3. The full details of the manufacturing steps are provided in the ESI†.

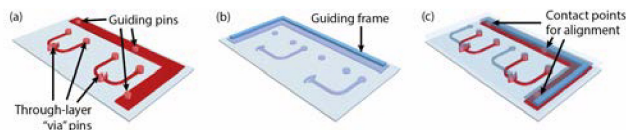


Fig. 2 Self-aligning molds using guiding structures. (a) Bottom mold containing guiding pins, bottom structures, and pins defining vias. (b) Top side molds containing guiding frame and top structures. (c) Bottom and top molds automatically aligned by contacting the guiding frames with the guiding pins. The valves, channels and the self-aligning features on the molds are oversized for illustrative purposes.

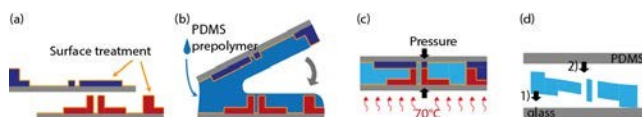


Fig. 3 Manufacturing process. Process flow for the manufacturing of double-sided molding of PDMS in three steps: (a) mold surface preparation, (b-c) PDMS device layer preparation, and (d) transfer bonding of PDMS layer from molds to assembly.

4 Evaluation Methods

4.1 Manufacturing tests

The manufacturing scheme was characterized in terms of its alignment accuracy between top and bottom features and miniaturization of thin vertical membranes and vertical interconnects (vias).

Alignment accuracy: The mold alignment accuracy was evaluated for PDMS structures fabricated in a mold composed of: a transparent glass micropatterned SU-8 top mold half; and a silicon / micropatterned SU-8 bottom mold half. For the remaining experiments, the manufacturing was performed as previously described²³, with two silicon based molds. In a first test, mold alignment relied on the self-aligning structures only, and in a second test, optical microscopy was used to fine-tune the alignment.

Downscaling limitations: The lower size limitations of this manufacturing method were investigated for two types of features: vertical vias, and vertical membranes. This was done by manufacturing arrays of PDMS grid structures with varying vias widths, and varying the membrane between the vias. The PDMS grids with varying vias sizes and membranes was defined by SU-8 molds with arrays of 120 μm tall square pillars, with increasing pillar widths and gaps, in increments of 10 μm . The SU-8 pillar arrays were coated with the mold coating previously described²³, covered with PDMS prepolymer, and clamped to a glass slide, with the same mold coating. The structures were clamped and cured with the recipe described in ESI† (chapter *Microstructured layer preparation*), demolded, and finally evaluated with microscopy to determine whether the vias and membranes had been successfully manufactured or not. This method is schematically depicted in Figure 4a.

4.2 Valve characterization setup

The valve ports were connected with tubing in the following manner: the flow inlet ports to a pressure-controlled container with deionized (DI) water at pressure P_{in} ; the flow outlet ports via a

flow sensor (ASL 1600-10, Sensirion AG, CH; sensor accuracy: for flow > 40 $\mu\text{l}/\text{min}$: 3.0 %, for flow < 40 $\mu\text{l}/\text{min}$: 0.15 %) to a waste container at atmospheric pressure P_{out} ; the pneumatic control ports to a piston pneumatic control pressure source at pressure P_{ctrl} . Pressure sensors were used to monitor the pressure in the DI water container (MTX2200DP, ELFA, Sweden; sensor accuracy: 0.25%) and at the pneumatic control source (SPD100G Smartec, ELFA, Sweden; sensor accuracy: 0.3%). The fluidic ports were able to withstand up to 300 kPa, hence forming a limitation to the experimental test parameters. The pressure-flow characteristics for the valves were measured as follows. The DI water container was pressurized between 0 and 50 kPa, with 12.5 kPa intervals, while the waste container was left at atmospheric pressure. During every interval, the pneumatic pressure was varied from 0 and 300 kPa, and the flow was measured with the flow sensor. The accuracy for regulating both the valve inlet pressure and the pneumatic control pressure is estimated at $\pm 5\%$. The readout error of the flow measurement data is estimated at $\pm 5 \mu\text{l}/\text{min}$. The “measured closing pressure” is defined as the minimum pneumatic pressure for which zero flow was measured. The “visual closing pressure” is defined as the minimum pneumatic pressure for which no gap between the membrane and the inner wall could be observed using microscopy imaging, similar as in previous work.^{11–13,25}

5 Results and discussion

5.1 Manufacturing results

Bell-valves and circle-valves were all successfully manufactured according to the process described.

Alignment accuracy: The measured bottom and top mold feature misalignment, m_r , was <25 μm when using self-aligning structures and <15 μm when using microscopy and transparent glass molds for alignment. Adjusting for the low-resolution printed plastic photomask ($r_p < 10 \mu\text{m}$), the error introduced during the alignment procedure, e_a , can be estimated as $e_a \approx \sqrt{m_r^2 - r_p^2}$, i.e. <23 μm and <11 μm , respectively, for self-aligning structures and microscopy assisted alignment. A limiting factor for alignment was relative movements of the molds during clamping, according to observations through glass molds. Previous double-sided molding methods^{26–28} feature one or two soft molds, vertical vias features of several hundred μm and require a manual alignment process during the patterning step which, according to Lucas et al.²⁶, limit the structure sizes to minimum 100 μm . Hence, our method provides a significant (nine-fold) alignment accuracy improvement.

Downscaling limitations: For 120 μm tall structures, Figure 4d shows the smallest successfully manufactured vertical membranes of thickness 20 μm (as defined by the distances between the SU-8 pillars) and Figure 4b shows the smallest successfully manufactured vias of width 30 μm , which results in a vertical vias density of ~ 30000 per cm^2 .

For vias 20 μm wide or smaller, a thin squeeze film of polymerized PDMS blocked the vias at the top (Figure 4c). A slight overhang of polymerized PDMS could be seen already at 30 μm (Figure 4b), although not enough to significantly block the vias.

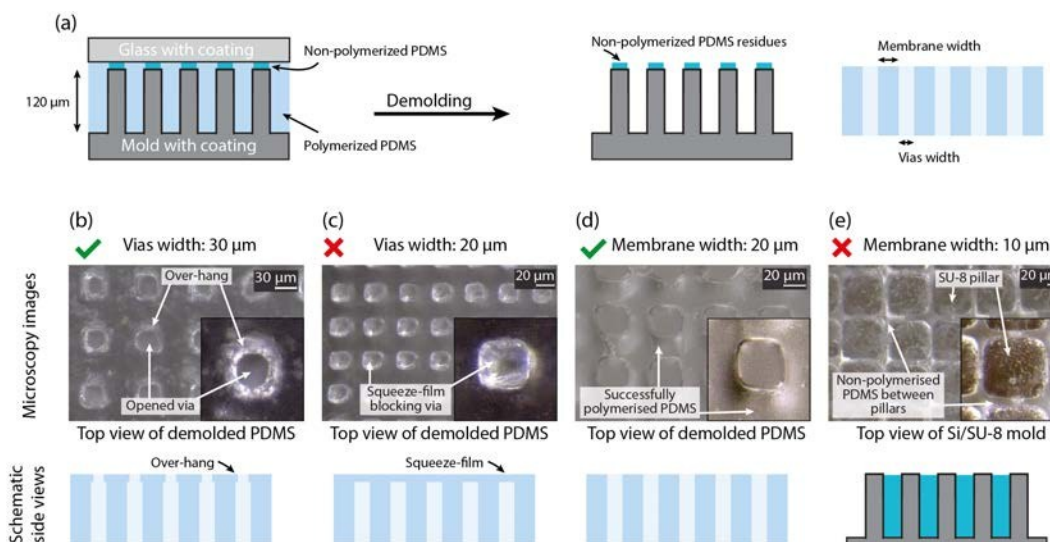


Fig. 4 Manufacturing Results. (a) Schematic side view of a successful instance of the manufacturing method used in this evaluation. (b-e) Microscopy images and schematic side views of the results from the smallest successfully manufactured vias (b), the biggest failing vias (c), the thinnest successfully manufactured membranes (d), and the biggest failing membrane (e). (b-e) The insets are zoom-ins with increased contrast

Attempting to manufacture membranes $10\mu\text{m}$ or smaller resulted in non-polymerized PDMS between the pillars in the SU-8 pillar mold (Fig. 4e), and hence, unsuccessful release of PDMS from the mold. However, there is room for optimization of the manufacturing parameters in order to achieve even thinner membranes.

Our new manufacturing technique enables several orders of magnitude higher vertical via density compared to standard hole punching^{11,25} and four-fold downscaling in lateral features compared to previously reported dual sided molding of PDMS^{26–28}. This provides significant gains in chip real estate.

Compared to horizontal membrane microfluidic devices, our novel manufacturing method comprises fewer steps and less stochastic processes than the standard manufacturing method of horizontal membrane microvalves, hence, potentially provides a more robust manufacturing method. See Table S3 in ESI† for a detailed comparison.

5.2 Valve characterization results

Fig. 5 shows images, measurement results, and data analysis from the valve characterization, and Table 1 summarizes the geometries tested, key performance results, and compare them to those of a few key references.

First, we actuated and imaged the valves with no liquid flow ($P_{in} = P_{out}$), observing closing of valves B2, B3, C2, and C3 (see Figure 5a and Figure S1 in the ESI†), while the largest valves (B1 and C1) did not close below the maximum available control pressure $P_{ctrl} \approx 300\text{kPa}$. This standard characterization technique, microscopy imaging from the top, is straightforward for horizontal membrane microvalves, but becomes challenging for vertical membrane microvalves at small effective valve heights, i.e. when the valve is near closing. Therefore, in addition to an indication of the visual closing pressure (see Table 1), we also pressurize the flow channels and measure the flow rate during membrane actuation for a more true characterization.

A first flow-test of the valves revealed that B2, B3 and C3, could be successfully closed leak-tight, whereas the other valve designs (B1, C1 and C2) were not leak tight at the maximum available control pressure $P_{ctrl} \approx 300\text{kPa}$. Valve B2 was classified differently in image-based and flow-based testing. Complete pressure-flow characteristics were only measured for the leak-tight valves.

Fig. 5c-e shows the measured pressure-flow characteristics data of the experimental setup for B2, B3 and C3 valves, i.e. the measured flow, Q , in function of the pneumatic control pressure, P_{ctrl} , for different values of the inlet port pressure, P_{in} . We can clearly see that valve B3 closes at the lowest control pressure.

The resulting flows are also influenced by the resistance of connecting channels. To obtain the characteristics of only the valves themselves, i.e. the measured flow, Q , in function of the pressure across the valve membrane, ΔP_m , and of the pressure drop across the valve channel, ΔP_v , we subtract the influence of inlet and outlet flow channels from measurements as detailed in the ESI†.

5.2.1 Valve closing pressures

The lowest pressure drop over the B2, B3 and C3 valve membranes that was required to close the valves were $\Delta P_{m,close,B2} = 188 \pm 10\text{kPa}$, $\Delta P_{m,close,B3} = 119 \pm 6\text{kPa}$, and $\Delta P_{m,close,C3} = 194 \pm 10\text{kPa}$ respectively.

The closing pressures of horizontal membrane microvalves have previously been compared to linear models of the membrane; as either a thick beam model, a thick spring model, or a thin spring model. Push-up horizontal membrane microvalves have shown to have closest resemblance to the thin spring model³⁰, and push-down horizontal membrane microvalves have shown to have closest resemblance to the thick spring model²⁵. Using the same models, the valves in this paper seem to have closest resemblance to the thin spring model, as they provide the best prediction for E_{PDMS} (see Table 2 for results and ESI† for calculations). These conclusions are from only three valves, but

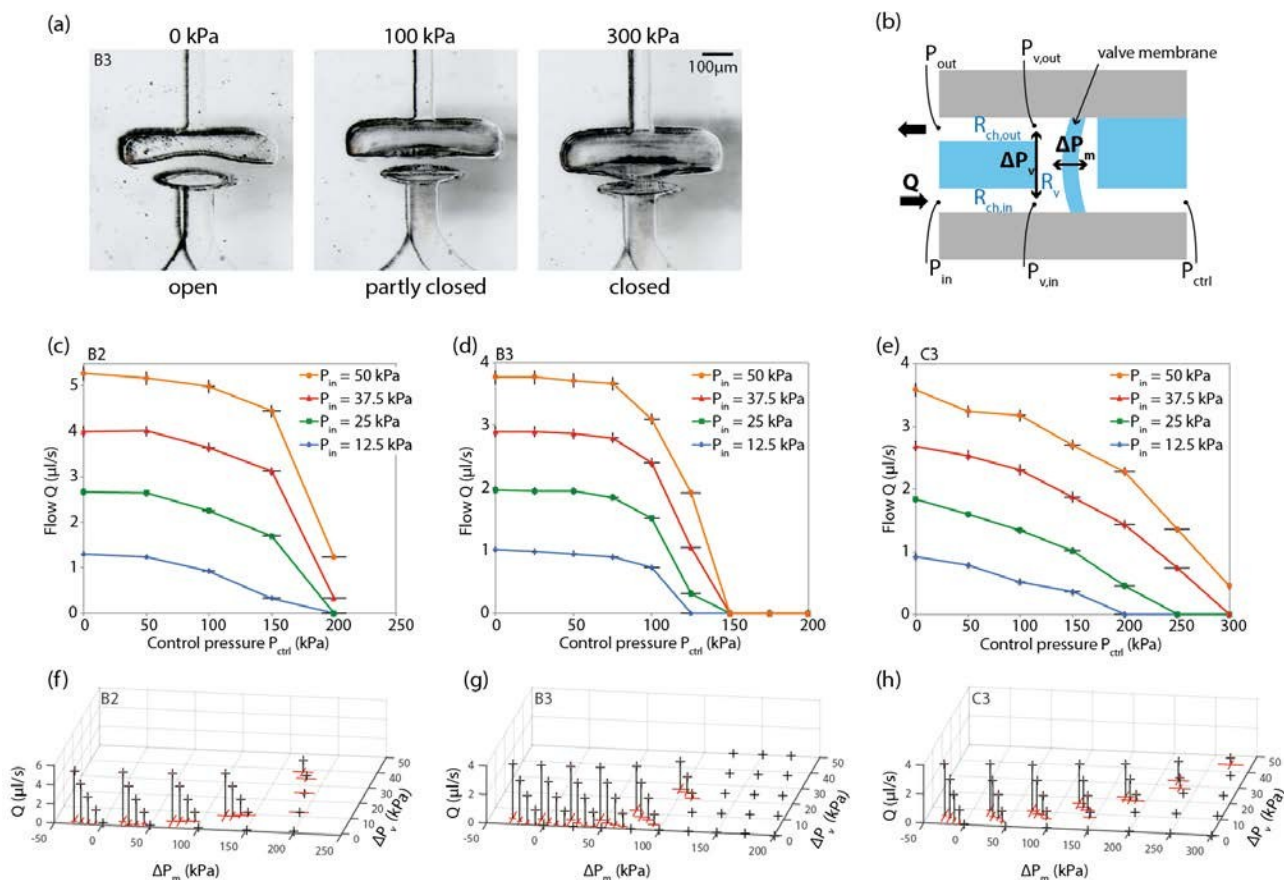


Fig. 5 Valve measurement results. (a) Microscopy images of the smallest bell valve (B3) at open state and at control pressures of 100 kPa and 300 kPa. (b) Overview sketch of parameters used in valve characterization and calculations (c-e) Measured pressure-flow characterization data of the B2, B3 and C3 valves in the experimental setup. The lines are added for eye guidance. (f-h) Calculated pressure-flow characteristics of the B2, B3 and C3 valves after subtracting the pressure drop in the inlet and outlet channels. Standard deviations, calculated from measurement uncertainties, are marked in black (c-e) and red (f-h).

the resemblance with push-down rather than push-up horizontal membrane microvalves is still interesting, as it can aid future design of vertical membrane microvalves to obtain lower closing pressures.

Neglecting the membrane geometries, but still assuming that the membranes behave as a linear spring, i.e. $\Delta P_m = k(h_v - h_{v,0})$, one can derive the spring constant of the membranes as $k = \frac{\Delta P_{m,close}}{h_{v,0}}$, i.e. $k_{B2} = 2.3 \text{ kPa}\mu\text{m}^{-1}$, $k_{B3} = 2.1 \text{ kPa}\mu\text{m}^{-1}$, and $k_{C3} = 3.3 \text{ kPa}\mu\text{m}^{-1}$. We can expect the membrane spring constant, k , to increase for increasing values of membrane thickness, t , and for decreasing values of the valve channel width, w : $k \propto t^\kappa / w^\delta$ with κ and δ exponential parameters > 0 . Indeed, whereas the membrane thickness, t , was the same for all vertical valve membranes, their spring constants $k_{B2} \approx k_{B3} < k_{C3}$ varied inversely with their width: $w_{B2} = w_{B3} > w_{C3}$.

Considering the valve membrane geometry, $k_{B1} \approx k_{B2}$ and $k_{C1} \approx k_{C2} \approx k_{C3}$, we can estimate the respective valve closing pressures for the B1, C1 and C2 valves to be $\Delta P_{m,close,B1} \approx 540 \text{ kPa}$, $\Delta P_{m,close,C1} \approx 400 \text{ kPa}$, and $\Delta P_{m,close,C2} \approx 330 \text{ kPa}$, all of which values are larger than the experimentally available control pressure, P_{ctrl} , which is in accordance with the fact that these valves could not be closed leak-tight in our setup.

Studying the valve behavior (Fig. 5f-h) it is apparent that the valves close with increasing ΔP_m , as expected. We can also note that the closing pressure increases with increasing valve pressure ΔP_v , most apparent in the C3 valve. As previous studies used $\Delta P_v = 0$, this is to the authors knowledge the first time report of the dependence of membrane microvalve closing pressure ΔP_m on the flow channel pressure drop ΔP_v . A previous study, using finite element simulation for very thin membranes accounting for both added P_{ctrl} and P_m , reported that an increase actuation pressure ($P_{ctrl,close}$) was equal to the increase in fluidic pressure (ΔP_v).³¹ This is not the case for C3, as the closing pressure increases far more than the increase in fluidic pressure. We can speculate that the increase in ΔP_v deforms the closed valve asymmetrically, forcing the closing point closer to the outlet channel, and hence demanding an increased extension of the membrane, at least along the L direction. This behavior would be more pronounced with increasing height, h_0 and thickness, t , and decreasing width, w which is accordance to the observations that this behavior is less pronounced in B2 and even less in B3. Modelling this behavior lays outside the scope of this work, but future microvalve modelling (and characterizations) of both vertical and horizontal membrane microvalves would benefit from taking the flow chan-

Table 1 Valve geometries, open valve properties, and summary of actuation results for the valves in this paper, two previous vertical membrane valves^{12,13}, and two previous horizontal membrane valves^{11,25}. The valve performance characteristics are rounded values. (Abbr.: n/a = not available, NP = not possible)

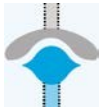






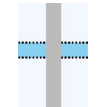


Valve type	B1	B2	B3	C1	C2	C3	V ¹³	V ¹²	H ¹¹	H ²⁵
Schematic cross-section										
Valve dimensions (μm)										
Height, h_0	236	78	56	120	100	60	20	30	10	65
Width, w	408	408	408	220	220	220	100	100	100	250
Length, L	140	140	140	140	140	140	250	50	100	250
Membrane thickness, t	70	70	70	70	70	70	14	20	30	15
Valve performance characteristics										
Visual closing pressure (kPa)	>300	~150	~100	>300	~150	~100	NP	NP	40	40
Measured closing pressure (kPa)	n/a	190	120	n/a	n/a	190	NP	NP	n/a	n/a
Open state flow ($\mu\text{l s}^{-1}$)	n/a	5.4	3.7	n/a	n/a	3.6	n/a	n/a	n/a	n/a
Fluidic conductance ($\mu\text{l Pa}^{-1} \text{s}^{-1}$)	400	20	5	80	40	9	0.1	2	0.01	7

Table 2 Linear model testing. Values for E_{PDMS} are calculated from valve closing pressures and valve geometries. E_{PDMS} is 549 kPa for PDMS(1:12.5) and 750 kPa for PDMS(1:10).²⁹ We use PDMS(1:10) but the effective ratio is expected to decrease due to initiator depletion in our manufacturing process.

Model for E_{PDMS} calculation	B2 (kPa)	B3 (kPa)	C3 (kPa)
Thick Beam	6014	5303	3451
Thick Spring	1350	1911	946
Thick Spring	557	576	559

nel pressure profile into account.

Comparing the Bell-valves and Circle-valves, we see that $\Delta P_{m,close,B2}$ and $\Delta P_{m,close,B3} < \Delta P_{m,close,C3}$. However, it is unclear whether this is caused by their bell shaped geometry or by their larger flow channel width, w_V (the three designs having similar values of flow channel height, h_{V0}). Interestingly, for the B2 and B3 valves, the difference between the measured and visual closing pressure is < 25%, whereas for the C2 and C3 valves, this (estimated) difference is approximately 50%. One could speculate that, indeed, the slowly tapering side ends of the bell valves make them more easily sealed off, whereas the higher angle at the edge of the circle valves results in leaky channel edges, even at high control pressures. This speculation finds support in previous work, e.g. by a finite element simulation demonstrating that the corners in a push-down horizontal membrane microvalve closes off at much higher pressures than the rest of the valve.³²

Compared to previously reported vertical membrane pneumatic actuators,^{12–14} our B2, B3 and C3 valves are the first vertical membrane valves reported that can be closed leak-tight.

Our vertical valves and previous horizontal valves with similar valve channel width, w , have similar footprint area, $A_{fp} \sim w^2$, which allows comparing their performance. Fordyce et al.²⁵ reports on a horizontal valve with geometries $w_H = 250 \mu\text{m}$, $h_H \approx 65 \mu\text{m}$, and $t_H \approx 15 \mu\text{m}$ with closing pressure $\Delta P_{m,close,H} \approx 40 \text{ kPa}$,

which can be compared to the C3 valve with $w_V = 220 \mu\text{m}$, $h_V = 60 \mu\text{m}$ and $t_V = 70 \mu\text{m}$ and closing pressure $P_{m,close,C3} \approx 200 \text{ kPa}$. The substantial higher closing pressure of the C3 valve compared to that of the horizontal valve can be attributed to the substantially higher membrane thickness: $t_V > t_H$. The thickness of horizontal PDMS membranes can be made small through layer spinning but may be practically limited by layer handling during manufacturing. Minimizing the thickness of vertical PDMS membranes is limited by the alignment accuracy of the molds: $t_{V,min} \sim e_a$. Thus, the manufacturing limitations for minimizing horizontal and vertical membrane thickness result in similar values: $t_{V,min} \approx t_{H,min}$. Therefore, although we only manufactured vertical membrane thicknesses $t_V \gg t_{V,min}$, there is no reason to believe that it would not be possible to manufacture vertical membrane valves with similar closing pressure as those for horizontal valves of similar size.

5.2.2 Valve pressure-flow characteristics

High fluidic resistance valves provide a limitation in flow throughput, especially when positioned in series in an integrated microfluidic network.

A first order geometrical analysis can be made to compare resistance in vertical and horizontal membrane valves. The channel height of horizontal valves is limited by the resist reflow process (traditionally $h_{H0,max,trad} \approx 30 \mu\text{m}$). The resist reflow process also suffers from large variations in channel height since it relies on melting photoresist. A recent systematic study trying to overcome this limitations have increased the possible height to $h_{H0,max} \approx 80 \mu\text{m}$, however for these heights, the variations are even larger. The height of vertical valves on the other hand, can be manufactured arbitrarily large, but is instead limited by the operational demand of the valve needing to be closed at least at the maximum available pneumatic pressure P_{ctrl} . Assuming large variations in open channel flow resistance is acceptable, for channel width values below $w \sim h_{H0,max}$, both vertical and horizontal valves can be designed with similar open state flow resis-

tance. For valve width values $w \gg h_{H0,max}$, however, the valve channel flow resistance of horizontal valves, $R_{v,H} \sim \frac{1}{wh_{H0,max}^3}$, becomes severely limited, whereas the flow resistance of the vertical valves, $R_{v,V} \sim \frac{1}{wh_{V0}^3}$, does not have such limitation, i.e. they can be freely increased in size without relative decrease in conductance.

We can also compare the conductance of the valves presented in literature. The magnitude order higher resistance of our inlet and outlet flow channels R_{ch} compare to that of the valve flow channel R_v , makes estimations of the open state valve channel flow resistance for measurements highly uncertain, and previous work has never characterized valve channel flow resistance by measurements. Instead, we calculate the flow resistance from the measured channel geometries in this paper, and the reported channel geometries of others (see Fig. 1 for results and ESI† for details on the calculations). Here we see that indeed, our valves provide an order of magnitude larger conductance than most previous valves, but similar conductance to that of the latest increase in resist reflow channel heights.

6 Conclusions

We designed, manufactured and evaluated the first vertical membrane PDMS microvalves that can be closed leak tight. A novel dual-sided mold manufacturing method enables the vertical valve manufacturing in a single micropatterned layer.

We demonstrated mold side alignment accuracies down to $23\mu\text{m}$ and $11\mu\text{m}$ for automatic self-alignment and manual microscopy assisted alignment procedures, respectively. Moreover, we successfully manufactured vertical wall structures as thin as $20\mu\text{m}$ and vertical vias as narrow as $30\mu\text{m}$, resulting in a vertical vias density of ~ 30000 per cm^2 . These results demonstrate four-fold improvement with respect to feature miniaturization for double sided molding of PDMS, compared to previous work. Additionally, our novel manufacturing method comprises fewer steps and is potentially more robust than the standard manufacturing method of horizontal membrane microvalves.

The manufacturing technique allows valves with unconventional flow channel cross sectional shapes to be designed and manufactured, which we used to realize vertical membrane microvalves with flow channels of two different geometries, bell and circle-valves. Furthermore, this manufacturing technology opens up more freedom to design the valve membrane in unconventional shapes, which together with new designs in flow channel cross section could potentially open up new functionalities in these types of pneumatic valves and actuators.

The manufacturing technologies for vertical membrane microvalves allow membrane thicknesses that are close to those of horizontal membrane microvalves, i.e. with similar closing pressure. The manufacturing of horizontal valves using the resist reflow technique, however, limits the valve channel height and therefore induces a larger open state valve channel resistance than that of our novel vertical valves for geometries with large width. We manufactured and characterized vertical valves with a (conservative) membrane thickness of $70\mu\text{m}$, and demonstrated leak tight closed valves at membrane pressure drops as low as 119kPa and open state flows of up to $5.4\mu\text{l s}^{-1}$.

The low fluidic resistances of these valves and alignment free manufacturing process makes these valves and their manufacturing suitable for high flowrate applications and large scale integration.

7 Acknowledgements

This work has been financially supported by the European Union through the seventh framework programme projects InTopSens (www.intopsens.eu).

References

- 1 T. Thorsen, S. J. Maerkl and S. R. Quake, *Science*, 2002, **298**, 580–584.
- 2 S. Tay, J. J. Hughey, T. K. Lee, T. Lipniacki, S. R. Quake and M. W. Covert, *Nature*, 2010, **466**, 267–271.
- 3 J. A. Weaver, J. Melin, D. Stark, S. R. Quake and M. A. Horowitz, *Nature Physics*, 2010, **6**, 218–223.
- 4 P. N. Duncan, S. Ahrar and E. E. Hui, *Lab on a Chip*, 2015, **15**, 1360–1365.
- 5 C. F. Carlborg, K. B. Gylfason, A. Kaźmierczak, F. Dortu, M. J. B. Polo, A. M. Catala, G. M. Kresbach, H. Sohlström, T. Moh, L. Vivien, J. Popplewell, G. Ronan, C. A. Barrios, G. Stemme and W. van der Wijngaart, *Lab on a Chip*, 2010, **10**, 281–290.
- 6 B. Zhang, Q. Dong, C. E. Korman, Z. Li and M. E. Zaghoul, *Scientific Reports*, 2013, **3**, year.
- 7 A. K. Au, H. Lai, B. R. Utela and A. Folch, *Micromachines*, 2011, **2**, 179–220.
- 8 K. W. Oh and C. H. Ahn, *Journal of Micromechanics and Microengineering*, 2006, **16**, R13.
- 9 J. P. Rolland, R. M. Van Dam, D. A. Schorzman, S. R. Quake and J. M. DeSimone, *Journal of the American Chemical Society*, 2004, **126**, 2322–2323.
- 10 J. Hansson, J. Karlsson, C. Carlborg, W. van der Wijngaart and T. Haraldsson, 2014 IEEE 27th International Conference on Micro Electro Mechanical Systems (MEMS), 2014, pp. 987–990.
- 11 M. A. Unger, H.-P. Chou, T. Thorsen, A. Scherer and S. R. Quake, *Science*, 2000, **288**, 113–116.
- 12 N. Sundararajan, D. Kim and A. A. Berlin, *Lab on a Chip*, 2005, **5**, 350–354.
- 13 A. R. Abate and D. A. Weitz, *Applied Physics Letters*, 2008, **92**, 243509.
- 14 S. J. Lee, J. C.-Y. Chan, K. J. Maung, E. Rezler and N. Sundararajan, *Journal of Micromechanics and Microengineering*, 2007, **17**, 843.
- 15 I. Doh and Y.-H. Cho, *Lab on a Chip*, 2009, **9**, 2070–2075.
- 16 A. R. Abate, M. B. Romanowsky, J. J. Agresti and D. A. Weitz, *Applied Physics Letters*, 2009, **94**, 023503.
- 17 A. Jamshaid, M. Igaki, D. H. Yoon, T. Sekiguchi and S. Shoji, *Micromachines*, 2013, **4**, 34–48.
- 18 D. H. Yoon, D. Wakui, A. Nakahara, T. Sekiguchi and S. Shoji, *RSC Advances*, 2014, **5**, 2070–2074.
- 19 G. Shao, Z. Cai, Z. Miao and W. Wang, *Microsystem Technolo-*

- gies, 2013, **19**, 1823–1828.
- 20 H. Kim, S. Lee and J. Kim, *Microfluidics and Nanofluidics*, 2012, **13**, 835–844.
- 21 J. M. Karlsson, T. Haraldsson, C. F. Carlborg and W. van der Wijngaart, *Journal of Micromechanics and Microengineering*, 2012, **22**, 075005.
- 22 J. M. Karlsson, T. Haraldsson, C. F. Carlborg, J. Hansson, A. Russom and W. van der Wijngaart, *Journal of Micromechanics and Microengineering*, 2012, **22**, 085009.
- 23 J. M. Karlsson, T. Haraldsson, C. F. Carlborg and W. van der Wijngaart, Proceedings of The Sixteenth International Conference on Miniaturized Systems for Chemistry and Life Sciences, Okinawa, Japan, 2012.
- 24 C. Carlborg, T. Haraldsson, M. Cornaglia, G. Stemme and W. van der Wijngaart, *Journal of Microelectromechanical Systems*, 2010, **19**, 1050–1057.
- 25 P. M. Fordyce, C. A. Diaz-Botia, J. L. DeRisi and R. Gomez-Sjoberg, *Lab on a Chip*, 2012, **12**, 4287–4295.
- 26 N. Lucas, S. Demming, A. Jordan, P. Sichler and S. Büttgenbach, *Journal of Micromechanics and Microengineering*, 2008, **18**, 075037.
- 27 A. Mata, E. J. Kim, C. A. Boehm, A. J. Fleischman, G. F. Muschler and S. Roy, *Biomaterials*, 2009, **30**, 4610–4617.
- 28 H.-H. Jeong, V. R. Yelleswarapu, S. Yadavali, D. Issadore and D. Lee, *Lab on a Chip*, 2015.
- 29 D. Armani, C. Liu and N. Aluru, Twelfth IEEE International Conference on Micro Electro Mechanical Systems, 1999. MEMS '99, 1999, pp. 222–227.
- 30 E. P. Kartalov, A. Scherer, S. R. Quake, C. R. Taylor and W. F. Anderson, *Journal of Applied Physics*, 2007, **101**, 064505.
- 31 A. Pandolfi and M. Ortiz, *Journal of Micromechanics and Microengineering*, 2007, **17**, 1487.
- 32 A. T. H. Lau, H. M. Yip, K. C. C. Ng, X. Cui and R. H. W. Lam, *Micromachines*, 2014, **5**, 50–65.